Chapter 2. Ground Penetrating Radar

The aim of Chapter 2 is to give an overview of the GPR basic principles and technology. A lot of definitions and often-used terms that will be used throughout the whole work will be explained here. Readers who are familiar with GPR and the demining application can skip parts of this chapter. Section 2.2.4 however can be interesting since a description of the hardware and the design parameters of a time domain GPR are given there. The description is far from complete, but it gives a good overview of the technological difficulties encountered in GPR systems.

2.1. Brief historical overview

The first use of electromagnetic pulses to determine the structure of buried features appeared in 1926 in the work of Hülsenbeck. He noted that any dielectric variation would also produce reflections and that the technique had advantages over seismic methods. The first ground penetrating radar survey to be reported was the determination of the depth of a glacier in 1929 by Stern [1] . Then the technology seemed to have lost interest until the late 1950's. From the beginning of the 1970's a lot of commercial applications using a GPR are mentioned in the literature, for example by Morey [2]. The systems used in that time were exclusively impulse time domain systems. The applications were mainly found in the domain of civil engineering: location of voids, containers, tunnels and rocks, detection of cables and tubes, measuring the thickness of ice and coal layers, probing the profiles of lakes and rivers, etc. From then until today, the range of applications has been growing steadily.

New applications as non-destructive testing, archaeology, roads and tunnel quality assessments, remote sensing, etc. appeared. In 1988, D. J. Daniels, D. J. Gunton and H. F. Scott published a tutorial paper entitled "Introduction to subsurface radar" [3], giving a good overview of the GPR technology at that time. In 1996, D. J. Daniels published his book on surface penetrating radar [4]. Many engineers and researchers who are active in the domain consider the tutorial paper and the book to be reference works. Every two years, an International Conference on GPR is organised. At the last two conferences, in 1998 and 2000, the author presented a paper describing his work (see List of Publications).

2.2. GPR principles

2.2.1. General

The operating principle of Ground Penetrating Radar is straightforward. A GPR couples EM waves in the ground and samples the backscattered echoes. An EM wave will be backscattered on any electrical parameter contrast in the ground, *i.e.* the permittivity e, the permeability m or the conductivity s. All these three macroscopic parameters are in general a function of frequency. In practice it will be primarily the contrast in permittivity, which leads to a reflection of the radiated EM waves. Earth materials are mostly nonmagnetic materials, having a relative magnetic permeability $m_r = m/m_0$ of 1, with $m_0 = 4p.10^{-7} H/m$ being the permeability of free space. This means that no contrast in permeability will be encountered. The change in conductivity primarily affects absorption of the radar signal by the medium. The variation in permittivity has the largest impact on the variation of the characteristic impedance of the medium (see also Section 2.2.3), so the encountered contrasts in permittivity e between materials in the ground will lead to a reflection.

The data recorded by a GPR are generally represented as a one, two or three dimensional dataset, denominated by the acoustic terminology A- B- and C-scans.

A-scan

A single waveform $b(x_i, y_j, t)$ recorded by a GPR, with the antennas at a given fixed position (x_i, y_j) is referred to as an A-scan (Fig. 2-1). The only variable is the time, which is related to the depth by the propagation velocity of the EM waves in the medium.
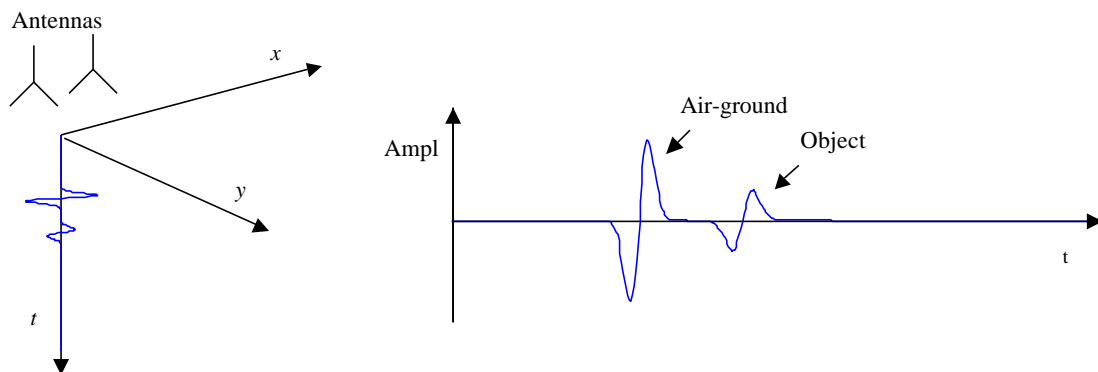

Fig. 2-1: Configuration and representation of an A-scan

B-scan

When moving the GPR antennas on a line along the x-axis, one can gather a set of A-scans, which form a two dimensional data set $b(x, y_j, t)$, called a B-scan (Fig. 2-2 (a)). When the amplitude of the received signal is represented by a colour scale (or grey-scale), a 2D image as shown in Fig. 2-2 (b) is obtained. The 2D image represents a vertical slice in the ground. The time axis or the related depth axis is usually pointed downwards.
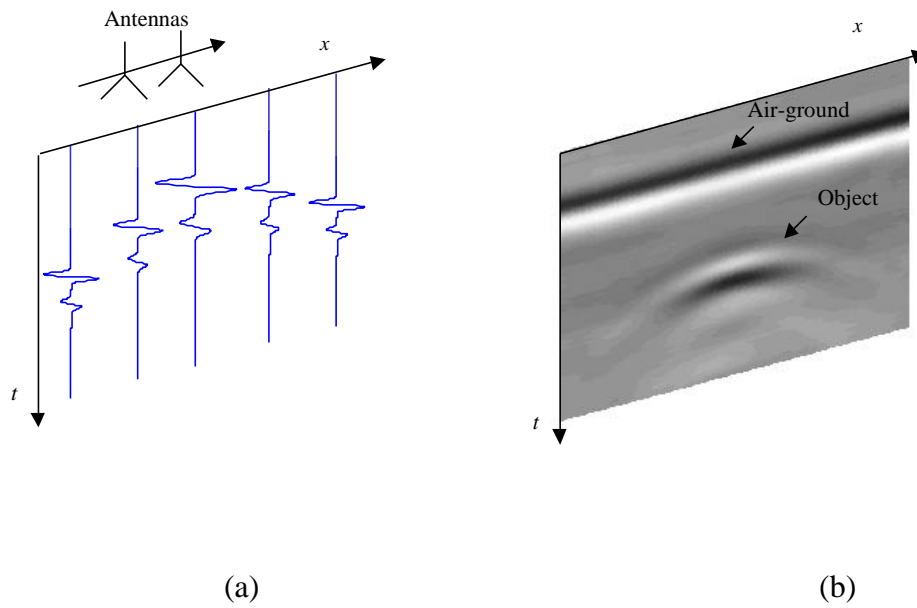
(a)   (b)

Fig. 2-2: (a) Multiple A-scans forming a B-scan

(b) Representation of a B-scan on a grey-scale

Reflections on a point scatterer located below the surface appear, due to the beamwidth of the transmitting and the receiving antenna, as **hyperbolic** structures in a B-scan. This can be easily verified, using the geometry shown in Fig. 2-3 (a). Suppose a homogeneous half-space with a propagation velocity equals v and the transmitting- and receiving antenna close to each other, so that they can be considered as one antenna (monostatic case). The co-ordinate system is represented on Fig. 2-3 (a). A point scatterer at a position $(0, z_0)$ in the half space, will be located by the antenna pair, situated in $(x,0)$ at a distance $\sqrt{x^2 + z_0^2}$. So in the recorded data $b(x,t)$, represented in Fig. 2-3 (b), the reflection on the point scatterer appears in each A-scan after a time

$$t = 2\sqrt{x^2 + z_0^2} \, / \, v \tag{2. 1}$$

Equation (2.1) represents a hyperbola with a vertical axis and an apex in $(0, 2z_0 / v)$. The shape of the hyperbola is function of the antenna configuration (monostatic, bi-

static), the depth of the point scatterer z_0 and the propagation velocity profile of the ground. The hyperbolic defocusing of an object can be corrected for in the data processing, this is called migration or SAR processing (see Chapter 7).
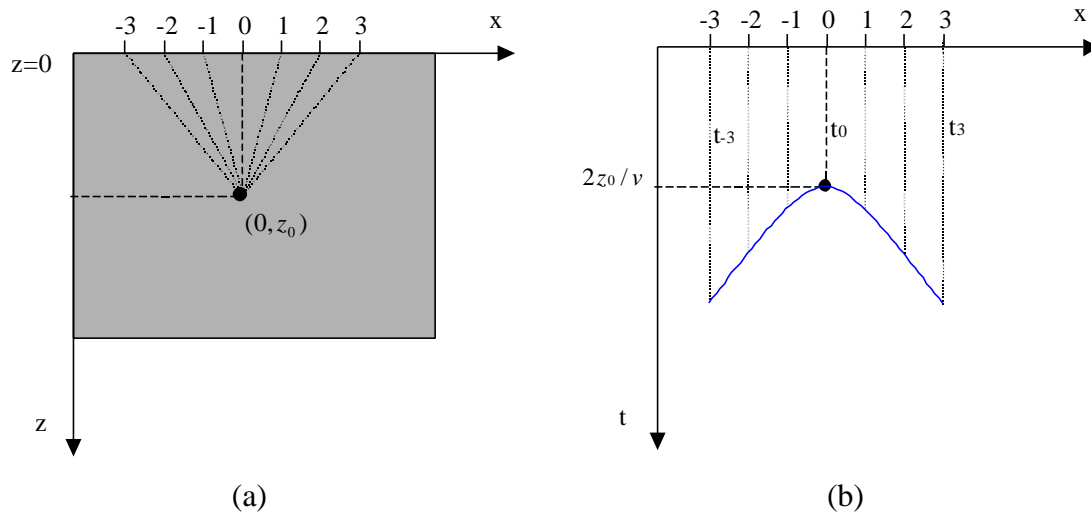

(a)   (b)

Fig. 2-3: (a) Point scatterer at position $(0, z_0)$, (b) recorded data $b(x,t)$

C-scan

Finally, when collecting multiple parallel B-scans or in other words, when moving the antenna over a (regular) grid in the xy-plane, a three dimensional data set $b(x, y, t)$ can be recorded, called a C-scan (Fig. 2-4). Usually a C-scan is represented as a two dimensional image by plotting the amplitudes of the recorded data at a given time t_i. The image $b(x, y, t_i)$ represents then a horizontal slice at a certain depth, parallel to the recording plane (Fig. 2-5). Nowadays, many user-software packages have integrated functions to plot directly three-dimensional representations of the recorded C-scans. In this case, an arbitrary cut in the 3-D volume (Fig. 2-6 (a)) or an iso-surface (surface with the same amplitude) is usually represented (Fig. 2-6 (b)).
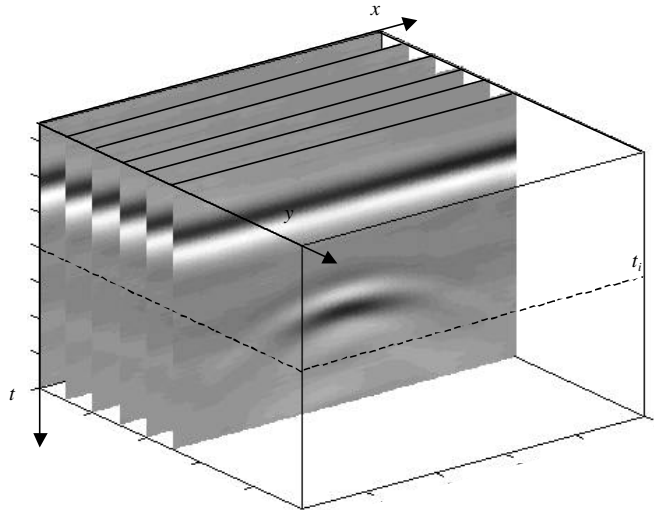
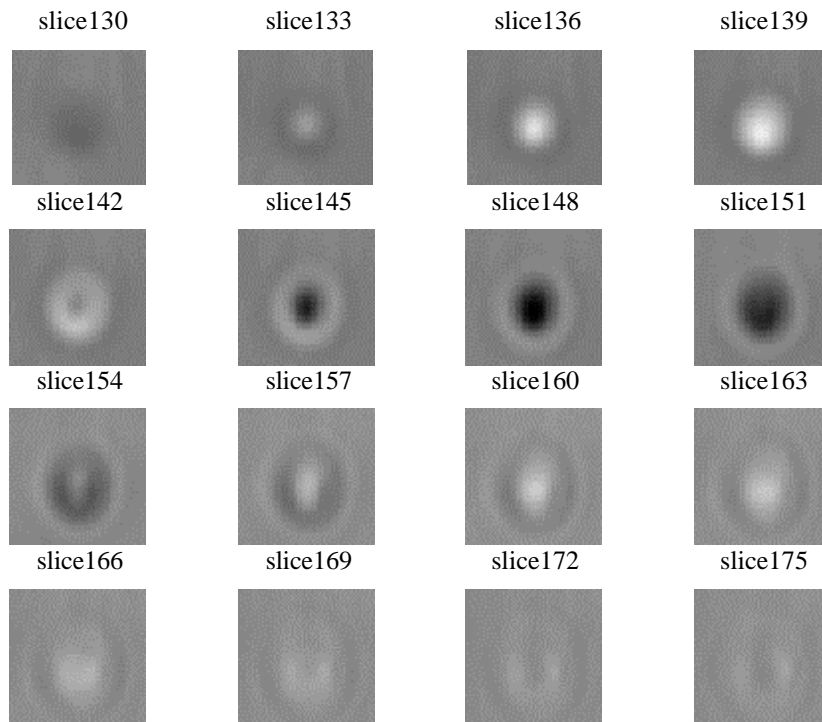**Fig. 2-4:** Multiple parallel B-scans forming a C-scan

Fig. 2-5: Representation of a C-scan by horizontal slices at different depths

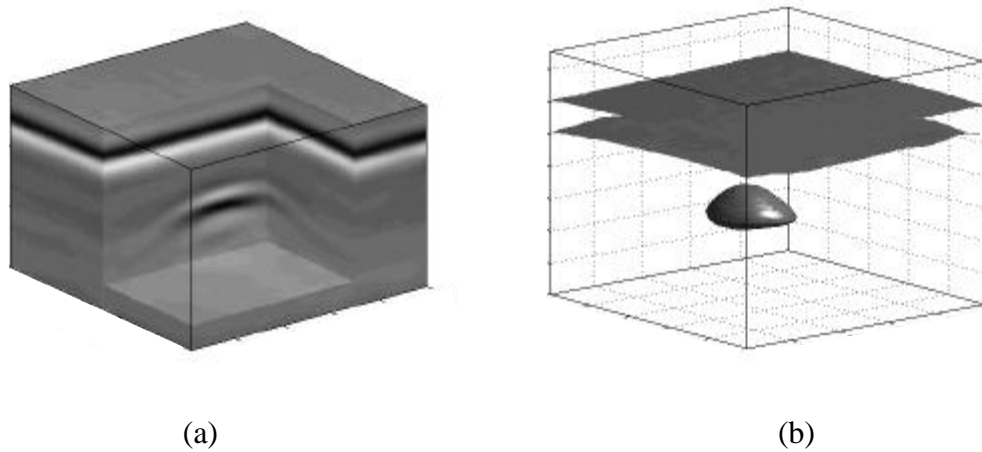(a)   (b)

Fig. 2-6: (a) Arbitrary cut in the 3-D volume, (b) iso-surface representation

2.2.2. Different types of GPR systems

Fig. 2-7 gives a schematic overview of the various possible types of GPR systems that exist today. GPR systems can be classified by the domain in which they work and by the type of modulation.
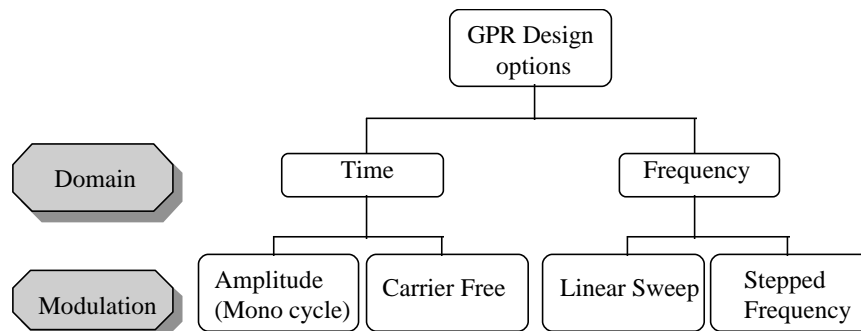

Fig. 2-7: Different types of GPR systems

The first family of GPR systems is the time domain GPR. The principle of a time domain GPR is to send a pulse at a given pulse repetition frequency (PRF) into the ground and then listen to the backscattered echoes. In the time domain GPR there are two major categories: the amplitude modulated and the carrier free GPR. The first one sends a pulse with a carrier frequency. This carrier frequency is modulated by a

(square) envelope. In order to achieve a good depth resolution it is important that the duration of the pulse is as short as possible. Therefore a monocycle is used. Most of the commercially available GPRs belong to this family. The central frequency of the monocycle can vary from some MHz up to some GHz as a function of the application. The 3dB bandwidth of the emitted pulse is equal to the central frequency f_c of the monocycle. Fig. 2-8 shows a monocycle of 1ns. The central frequency and the 3dB bandwidth is 1 GHz.
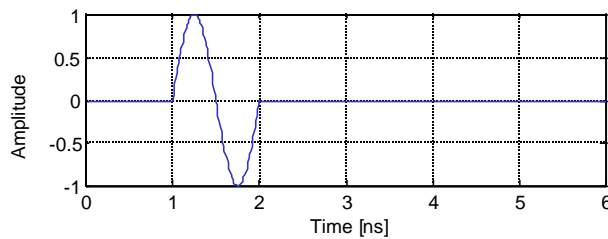

Fig. 2-8: A monocycle of 1ns

The need for larger bandwidth has led to the development of a second category of time domain GPR: the carrier-free GPR. The pulse sent by the GPR has no carrier. The width of the carrier free pulse is of the order of some 100 ps. The shape of the pulse can vary, but typically a Gaussian pulse is used. The carrier-free radar is also called an **UWB GPR** (Ultra-WideBand) because of the large bandwidth. The use of the term UWB is slightly different than in conventional air radar systems. A radar system is defined by the Defence Advanced Research Project Agency's (DARPA) [5] to be UWB if its fractional bandwidth is larger than 25%. The fractional bandwidth BW of a system, also defined by DARPA, is given by

$$BW = \frac{2(f_{max} - f_{min})}{f_{max} + f_{min}} 100\% \tag{2. 2}$$

where f_{max} and f_{min} are the higher and lower limits of the frequency range within which some specified fraction (90-99%) of the total signal energy lies. With this definition, almost all the GPR systems would be UWB. There is no alternative definition for GPR systems, but it is generally accepted that UWB GPR must have a

fractional bandwidth larger than 100%. In this work we will hold to this definition. So UWB GPRs have a fractional bandwidth larger than 100%.

The block diagram of a time domain GPR (Fig. 2-9) is much less complicated than the classic pulsed air radar. In the diagram one can see four major parts: the transmitter, the receiver, the timing circuit and the processing part. The fast sampling in the receiver part is done with a sequential sampler (see Section 2.2.4).
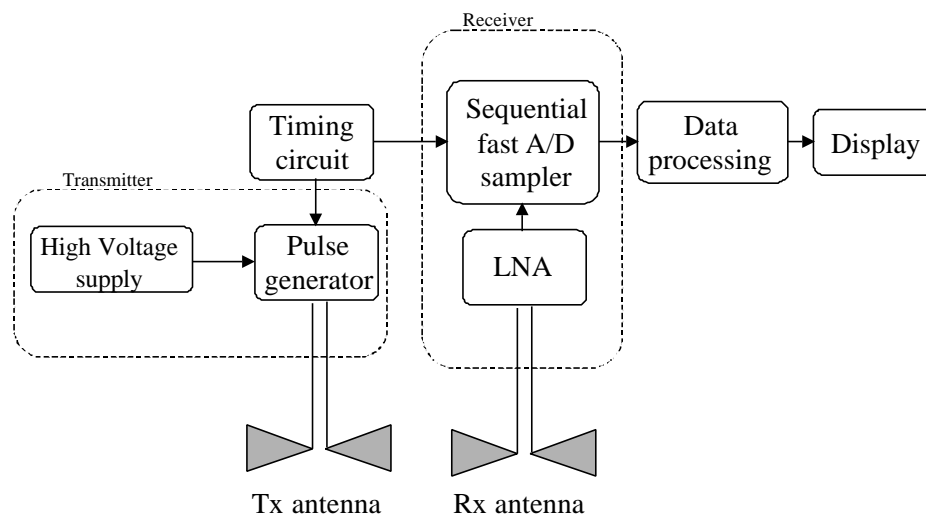

Fig. 2-9: Block diagram of a time domain GPR

The majority of the GPR systems use a time domain waveform, although the last decades GPRs are also developed in the frequency domain. In the frequency domain there are also two possible modulation types: either the continuous wave is frequency modulated with a linear sweep, named FMCW GPR, or the frequency of the continuous wave changes in fixed steps, called stepped frequency GPR.

A FMCW system transmits a continuously changing carrier frequency by means of a VCO over a chosen frequency range. The frequency sweeps according to a sawtooth or a triangular function within a certain dwell time. After reception, the backscattered wave is mixed with the emitted wave. The difference in frequency between the transmitted and received wave is a function of the depth of the target. A major limitation of the FMCW radar is the poor dynamic range of the system. The FMCW radar is receiving signals at the same time as it is transmitting. The leakage signal

between the antennas can mask the smaller backscattered signals. Therefore the development of FMCW for the GPR application was abandoned and from the late 1970's on, more attention has gone to the stepped-frequency radar.

A stepped frequency GPR uses a frequency synthesiser to step through a range of frequencies equally spaced by an interval Δf. At each frequency, a CW is radiated with a high stability and mixed with the received signal using a quadrature mixer. The I and Q baseband signals can be sampled using high precision, low speed A/D converters. This means that for each frequency, the amplitude and phase of the received signal is compared with the transmitted signal. A good overview of this technique is found in [6]. The stepped frequency radar is shown schematically in Fig. 2-10.
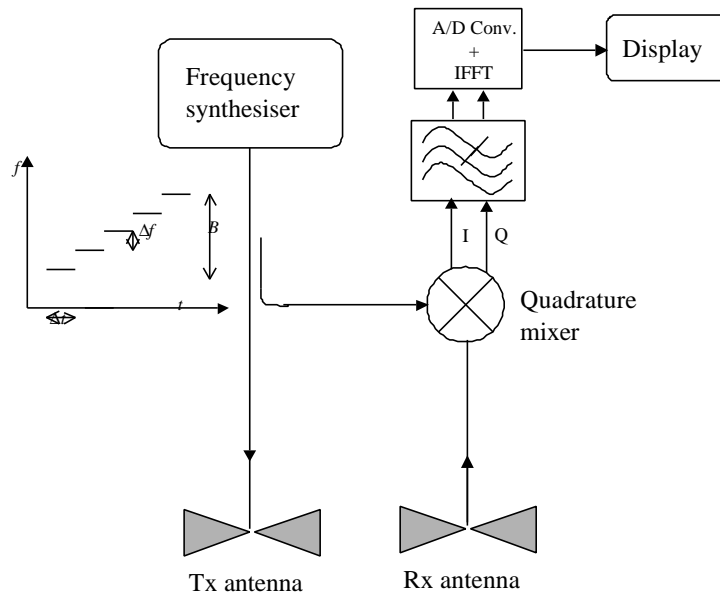

Fig. 2-10: Block diagram of a stepped frequency GPR

The transmitted CW signal of a stepped frequency radar at frequency f can be written as

$$E_t(f) = E_t e^{-j2\pi ft} \tag{2.3}$$

When only one object is present, the received signal is

$$E_r(f) = |\Gamma_0| E_{r0} e^{-j(2\pi ft - 2R\beta - f_0)}$$
(2. 4)

where $|\Gamma_0| e^{jf_0}$ is the reflection coefficient of the target, R the distance between the antennas and the target and β the phase constant of the medium. E_{r0} is a phasor that contains all the modifications of the transmitted signal, except the phase change related to the distance and the reflection on the object, so it contains for example the free-space loss $1/R$ and the losses in the ground. The coherent receiver measures the received signal with respect to the transmitted signal. If multiple reflectors are present, the received signal will be a combination of these different reflections. This is repeated for all frequencies. The measured frequency data can afterwards be transformed to an equivalent time domain representation by an inverse fast Fourier transformation (IFFT).

The stepped frequency GPR has some advantages over a time domain GPR. Its dynamic range can be designed to be greater and a narrow band coherent receiver can be used. Further, for two systems yielding the same bandwidth, the S/N ratio will be much higher for the stepped frequency system, because the mean radiated power radiated by a stepped frequency GPR is much higher compared to the mean radiated power radiated by a time domain GPR. The disadvantage of the stepped frequency GPR is the acquisition time. A stepped frequency GPR has to step trough a number of frequencies for an acquisition of one A-Scan and for each A-scan an IFFT has to be calculated. With today's technology, the time issue becomes less of a problem. The University of Queensland (Australia) [6] has developed a stepped frequency GPR that only needs 3.6 ms for the acquisition of one A-scan. Impulse systems often have to average several A-scans to enhance their dynamic range, so that the difference in acquisition time is negligible.

2.2.3. Propagation in lossy dielectric material

For a good understanding of the physics behind GPR, it is indispensable to study the EM wave propagation in a lossy dielectric material. Without loss of generality, the study is limited to the propagation of uniform plane waves. More complicated wave fronts can always be described as a combination of plane waves.

Earth materials, and soils in particular, can be considered as a conductive (lossy) dielectric medium. Maxwell's equations describing the wave propagation in a conductive dielectric are

$$\nabla \times \vec{E} = -\frac{\partial(\vec{B})}{\partial t} \tag{2. 5}$$

$$\nabla \times \vec{H} = \vec{J} + \frac{\partial \vec{D}}{\partial t} \tag{2. 6}$$

In harmonic regime, equation (2.5) and (2.6) can be written as

$$\nabla \times \vec{E} = -j\omega\mu\vec{H} \tag{2. 7}$$

$$\nabla \times \vec{H} = (\sigma + j\omega\varepsilon)\vec{E} \tag{2. 8}$$

with $\sigma = \sigma' - j\sigma''$ the complex conductivity of the medium, describing how well the medium conducts electric current. At higher frequencies the response time can become significant, resulting in an out of phase component. The imaginary part of the conductivity is related to this out-of-phase polarisation component and is usually small at most radar frequencies.

$\varepsilon = \varepsilon' - j\varepsilon''$ the complex permittivity. The real part of the permittivity ε' is a measure of the ability of the medium to be polarised under an electric field. For the high frequency range the dipoles can not follow the fast change in magnitude of the electric field, and the polarisation will be out of phase, there is a relaxation phenomena. The imaginary part of the permittivity relates to this out-of-phase polarisation component and can usually not be neglected at most radar frequencies.

μ the permeability of the medium. If the material is non-ferrous, the approximation $\mu \approx \mu_0$ is valid.

In equation (2.8) we notice that for conductive dielectrics, the macroscopic parameters σ and ε always occur in the combination $\sigma + j\omega\varepsilon$. Splitting up the two parameters in their real and imaginary part, this combination can be rewritten as

$$\sigma + j\omega\varepsilon = (\sigma' + \omega\varepsilon'') + j\omega(\varepsilon' - \frac{\sigma''}{\omega}) \qquad (2.9)$$

$$= \sigma_e + j\omega\varepsilon_e \qquad (2.10)$$

where $\sigma_e = \sigma' + \omega\varepsilon''$ is defined as the real effective conductivity,

$\varepsilon_e = \varepsilon' - \sigma''/\omega$ is defined as the real effective permittivity.

The real effective conductivity determines a current in phase with the electric field and the real effective permittivity is related to a current out of phase with the electric field.

It is also useful to define ε^*, the complex apparent permittivity, as

$$j\omega\varepsilon^* = \sigma_e + j\omega\varepsilon_e \qquad (2.11)$$

and the loss tangent $\tan d$ as

$$\tan d = \frac{s_e}{we_e} \tag{2.12}$$

By substituting (2.12) in (2.11), the complex apparent permittivity can be expressed as a function of the loss tangent:

$$e^* = e_e(1 - j\tan d) \tag{2.13}$$

Thanks to the definition of the complex apparent permittivity, equation (2.8) can be written as

$$\nabla \times \vec{H} = jwe^*\vec{E} \tag{2.14}$$

By substitution of (2.7) in (2.14), the wave equation describing the electric field wave propagation in a lossy dielectric medium is found as

$$\nabla^2\vec{E} + e^* m w^2 \vec{E} = 0 \tag{2.15}$$

The solution of equation (2.15) representing an harmonic plane wave, propagating in the direction $\vec{k}$, is

$$\vec{E} = \vec{E}_0 e^{-j\vec{k}\vec{r}} \tag{2.16}$$

with the wave number $k = |\vec{k}|$ given by

$$k = w\sqrt{e^* m} \qquad (2.\,17)$$

The wave number k is complex and may be separated into real and imaginary parts:

$$jk = a + jb \qquad (2.\,18)$$

The plane wave solution (2.16) can be written as

$$\vec{E} = \vec{E}_0 e^{-a\vec{r}} e^{-jb\vec{r}} \qquad (2.\,19)$$

The first exponential term represents the attenuation of the plane wave in a lossy medium. The rate is specified by a, the *attenuation constant.* The second exponential term represents the propagation, the phase is controlled by the *phase constant b.* The constants are given by

$$a = w\sqrt{me_e}\sqrt{0.5\left(\sqrt{1+tg^2 d}-1\right)} \text{ , the attenuation constant (Np/m) of the medium} \qquad (2.\,20)$$

$$b = w\sqrt{me_e}\sqrt{0.5\left(\sqrt{1+tg^2 d}+1\right)} \text{ , the phase constant (rad/m)} \qquad (2.\,21)$$

It can be seen in (2.20) that the attenuation of the EM wave in a conductive medium is due to both the conductive and dielectric effects. In table 2.1 the attenuation, the loss tangent and the relative permittivity of some soil types, measured in the scope of the HUDEM project are given for a frequency of 2 GHz [7]. Similar tables, reporting the attenuation and relative permittivity of various materials and soils at radar frequencies can be found in [4][8].

Material	Relative permittivity	Loss tangent	Attenuation [dB/m]
Air	1	0	0
Sandy soil , 0% of moisture content	2.55	0.004	1.22
Sandy soil, 15% of moisture content	11.58	0.087	54.06
Loamy soil, 0% of moisture content	2.82	0.018	5.38
Loamy soil, 15% of moisture content	11.13	0.09	54.82

Table 2.1: The relative permittivity, loss tangent and attenuation of some soil types

The complex parameters e and s and hence a and b are primarily function of frequency and water content. To illustrate this, we show in Fig. 2-11 the attenuation constant of sand as a function of frequency in the range from 2 GHz to 18 GHz and the water content expressed in a percentage of volume. The measurements were performed by the University of Louvain-la-Neuve in the scope of the HUDEM project [7]. It can be seen that the attenuation in the soil increases dramatically with frequency. Hence the choice of the frequency band of a GPR system will strongly influence the maximum penetration depth of the system.
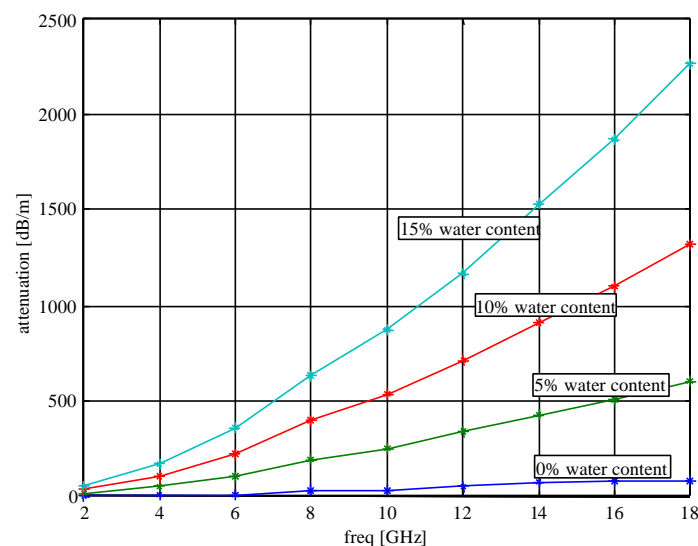

Fig. 2-11: The attenuation constant of sand as a function of frequency and water content.

Approximations

In the literature, many approximations are found to simplify the parameters that characterise the propagation of EM waves in a lossy media. The approximations depend on the kind of application and the frequency band of interest. For GPRs, *i.e.* propagation in earth material and for frequencies in the range from MHz to some GHz, the following approximations are generally accepted.

1. The influence of the imaginary part of the conductivity can be neglected with respect to the influence of the real part of the permittivity, or

$$e' >> \frac{s''}{w} \tag{2.22}$$

In other words, the conductivity of the soil is taken to be the conductivity at DC: $s = s_{DC}$. This means that the effective conductivity and effective permittivity may be assumed to be

$$\begin{cases} s_e = s_{DC} + we'' \\ e_e = e' \end{cases} \tag{2.23}$$

2. Earth materials are considered to be a low-loss dielectric, having a small loss tangent:

$$(\tan d)^2 << 1 \tag{2.24}$$

This is usually the case if the moisture content of the soil is not too high.

In this research we will consequently use these two approximations. Under these approximations, the attenuation constant and the phase constant can be simplified to

$$a = w\sqrt{me'}\,\frac{\tan d}{2} \qquad\qquad (2.\,25)$$

$$b = w\sqrt{me'} \qquad\qquad (2.\,26)$$

The propagation velocity v of the wave is related to the phase constant by

$$v = \frac{w}{b} \qquad\qquad (2.\,27)$$

Using the two approximations (2.22) and (2.24), the velocity of EM waves in earth material can be expressed as

$$v \approx \frac{c}{\sqrt{e'_r}} \qquad\qquad (2.\,28)$$

with c the propagation velocity in free space and e'_r the real part of the relative permittivity. Expression (2.28) is generally accepted in GPR applications and is even accurate for soils with higher losses (like for water saturated soils) as far as $\tan d < 1$ [4].

The constant Q model

Q or quality factor, is defined by IEEE Std. 145-1983 as the ratio of $2p$ times the energy stored to the energy radiated and dissipated per cycle. In Fig. 2-12 (a) and (b) we show the attenuation coefficient of 2 different types of soils, each type with a water content of 5% and 10 %. Subplot (a) represent the attenuation in sand, (b) represents the attenuation in a loamy soil. The lines (in green) fitted through the measured points suggest that the attenuation in the soils is almost linear with frequency in a large frequency band. It is this property that is explored in the constant Q model.
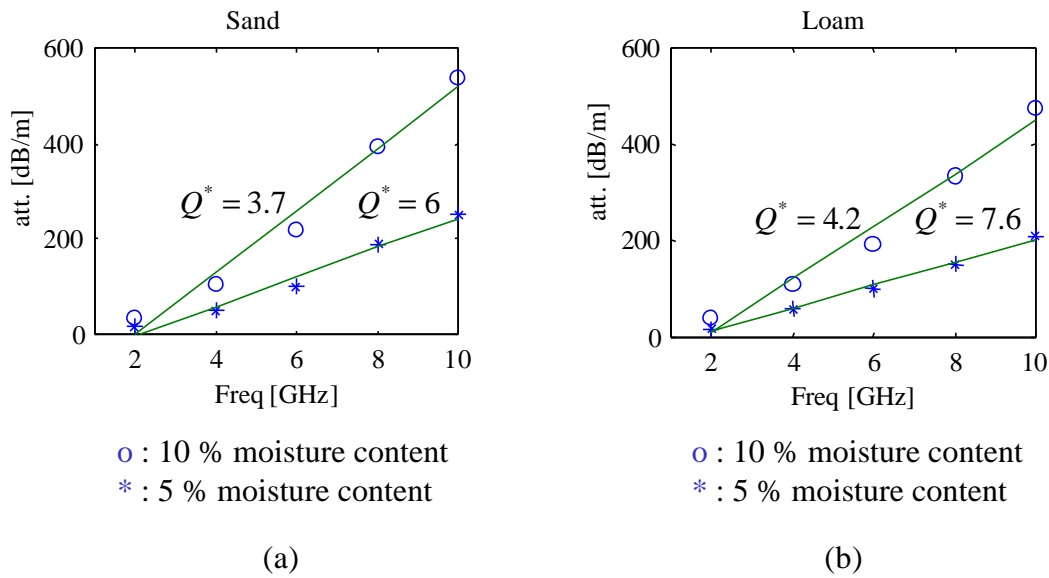
Fig. 2-12: Attenuation in (a) sand and (b) loamy soil versus frequency, measurements performed at UCL

If the attenuation is almost linear with frequency, the attenuation and distortion of EM waves in the material can be successfully described by the constant Q model [6][9]. For seismic waves, Q has been found to be frequency independent over a large frequency band and is given by

$$Q = \frac{w}{2v\boldsymbol{a}} \tag{2. 29}$$

with $\boldsymbol{a}$ the attenuation coefficient and v the propagation velocity. This implies that the attenuation is linear with frequency. In [9] it is suggested that this property can be extended to EM waves in earth materials with low losses and that the definition of Q in (2.29) holds in this specific case. In [9] they also define a parameter Q^*, which is a generalisation of the Q parameter. The Q^* parameter describes the gradient of the best fit line for each attenuation curve, where the attenuation at zero frequency can be non-zero. In Fig. 2-12 the Q^* factor is given for the different lines that are fitted through the measured attenuation points. For earth materials, the Q^* factor is usually

in the range from 2 to 30. The Q factor is related to the electric parameters of the soil. Combining (2.29) with (2.25) results in

$$Q = \frac{w}{2v\boldsymbol{a}} = \frac{w}{2v(w \tan \boldsymbol{d} / 2v)} = \frac{1}{\tan \boldsymbol{d}} \tag{2.30}$$

As a consequence, it is assumed that for constant Q the loss tangent is independent of frequency and that the real part of the permittivity $\boldsymbol{e}'$ is independent of frequency (because $\boldsymbol{a}$ is linear with frequency). The latter assumption is generally true for radar frequencies. In the measurements on different soils we noticed however that the first assumption ($\tan \boldsymbol{d}$ independent of frequency) is not always correct, certainly not when soils have a higher water content. Anyway, the most important observation is that the frequency dependence of all the electrical parameters together produces a form of attenuation that is nearly linear with frequency.

The constant Q model provides a mechanism to describe the attenuation and the dispersion of EM waves in earth material by one single parameter Q. The attenuation constant and the phase constant are linear with frequency and given by

$$\boldsymbol{a} = \frac{\sqrt{\boldsymbol{me}'}}{2Q} w \tag{2.31}$$

$$\boldsymbol{b} = 2\boldsymbol{a}Q \tag{2.32}$$

We introduce the constant Q model in this section, but we will use it in Chapter 5. It allows us to calculate an analytical expression of the impulse response of the ground, *i.e.* an impulse response that describes the propagation of an EM wave through a lossy ground over a certain distance.

Table 2.2 summarises the most important terms and ground properties that are introduced in this section. In the last column, the approximated expressions used in this work are given.

Term		Expression	Approximation
Permittivity of free space	$\boldsymbol{e}_0$	$\approx 8.85 * 10^{-12} \, F/m$	
Permeability of free space	$\boldsymbol{m}_0$	$= 4\boldsymbol{p} * 10^{-7} \, H/m$	
Complex dielectric permittivity	$\boldsymbol{e}$	$= \boldsymbol{e}' - j\boldsymbol{e}''$	
Real part of dielectric constant	$\boldsymbol{e}'$		constant with freq.
Imag. part of dielectric constant	$\boldsymbol{e}''$		
Complex conductivity	$\boldsymbol{s}$	$= \boldsymbol{s}' - j\boldsymbol{s}''$	
Real part of conductivity	$\boldsymbol{s}'$		$= \boldsymbol{s}_{DC}$
Imag. part of conductivity	$\boldsymbol{s}''$		$= 0$
Magnetic permeability	$\boldsymbol{m}$		$= \boldsymbol{m}_0$ for earth mat.
Real effective conductivity	$\boldsymbol{s}_e$	$= \boldsymbol{s}' + w\boldsymbol{e}''$	
Real effective permittivity	$\boldsymbol{e}_e$	$= \boldsymbol{e}' - \boldsymbol{s}''/w$	$= \boldsymbol{e}'$
Loss tangent	$\tan \boldsymbol{d}$	$= \dfrac{\boldsymbol{s}_e}{w\boldsymbol{e}_e}$	$= \dfrac{\boldsymbol{s}_{DC} + w\boldsymbol{e}''}{w\boldsymbol{e}'}$
Complex apparent permittivity	$\boldsymbol{e}^*$	$= \boldsymbol{e}_e(1 - j\tan \boldsymbol{d})$	$= \boldsymbol{e}'(1 - j\tan \boldsymbol{d})$
Complex wave number	k	$= w\sqrt{\boldsymbol{e}^* \boldsymbol{m}} = \boldsymbol{b} - j\boldsymbol{a}$	
Attenuation constant	$\boldsymbol{a}$	$= w\sqrt{\boldsymbol{m}\boldsymbol{e}_e}\sqrt{0.5(\sqrt{1 + \tan^2 \boldsymbol{d}} - 1)}$	$= w\sqrt{\boldsymbol{m}\boldsymbol{e}'}\dfrac{\tan \boldsymbol{d}}{2}$
Phase constant	$\boldsymbol{b}$	$= w\sqrt{\boldsymbol{m}\boldsymbol{e}_e}\sqrt{0.5(\sqrt{1 + \tan^2 \boldsymbol{d}} + 1)}$	$= w\sqrt{\boldsymbol{m}\boldsymbol{e}'}$
Velocity in free space	c	$\approx 3.10^8$	
Phase velocity	v	$= w/\boldsymbol{b}$	$= \dfrac{1}{\sqrt{\boldsymbol{m}\boldsymbol{e}'}} = \dfrac{c}{\sqrt{\boldsymbol{e}_r'}}$

Table 2.2: Summary of the most important terms and ground properties

2.2.4. Impulse GPR design parameters

In Section 2.2.2, an overview of the different types of GPR systems was given. In this section we will describe the family of the time domain GPR into some more detail. A general overview of the technology for the transmitter and receiver, as well as some system design parameters will be discussed. In Fig. 2-13 we repeat the block diagram of a time domain GPR. Besides the data processing and display we distinguish 3 parts: the transmitter, the receiver and the timing circuit which triggers both the transmitter and receiver.
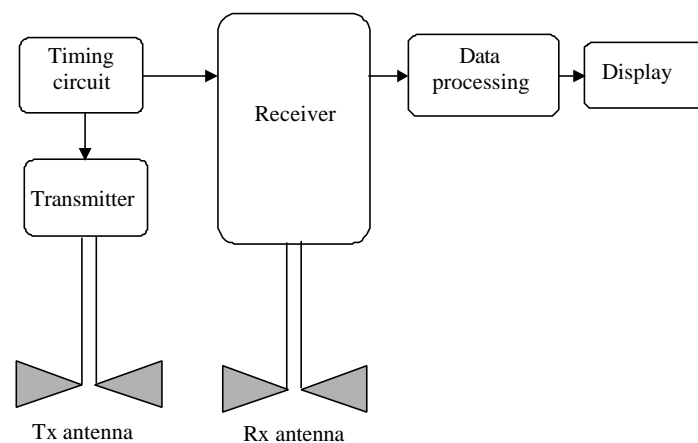

Fig. 2-13: Block diagram of a time domain GPR

Transmitter

The transmitter is a pulse generator, producing short transient pulses with a certain periodicity. This periodicity is called the pulse repetition frequency (PRF). The shape of the pulse is usually a monocycle or a Gaussian pulse, but other shapes like a derivative of a Gaussian pulse or even a step are possible. The impulse generator is generally based on the technique of rapid discharge of stored energy in a capacitor or short transmission line. A block diagram of the principle is shown in Fig. 2-14.
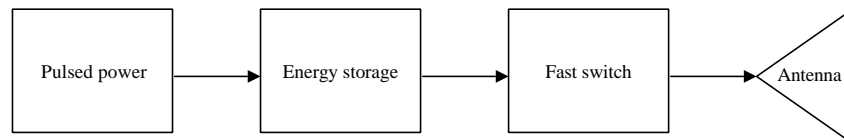
Fig. 2-14: Block diagram of pulse generator

The fast switch is an important component in the diagram. The most commonly used technologies for fast switches in GPR are semiconductor switches based on avalanche transistors, step-recovery diodes (SRD) or a combination of these two. In the latter, the SRD is then used to enhance the rise-time of the transition. The avalanche transistor and the SRD are characterised by a high figure of merit in the order of 100-1000 V/ns. The figure of merit is defined as the maximum variation of a signal amplitude per unit of time. It is this characteristic that is needed to generate a transition with a very short rise-time. Fig. 2-15 shows a simplified schematic of a step generator using a transmission line to store the energy and an avalanche transistor as a fast switch [10]. The driving pulse will put the avalanche transistor in a conductive stage so that the transmission line will discharge over the output resistor R_L.
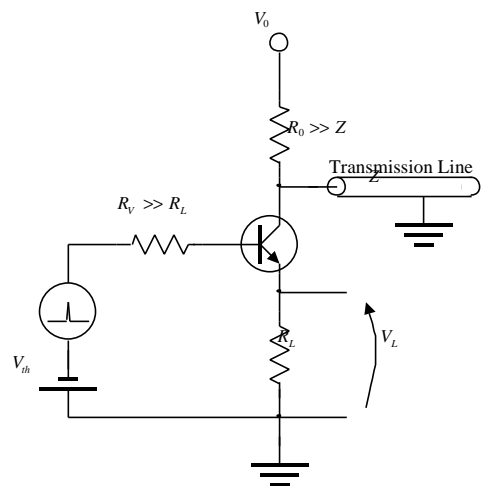

Fig. 2-15: Simplified schematic of a step generator

The maximum amplitude of the waveform generated by a pulse generator decreases with the pulse duration or rise time. Typical values for GPRs are between 20 V and 100 V. The transmitter receives an external trigger from a timing circuit. The storage of the energy or the recovery of the fast switch can take a certain time, so in general

the transmitter will limit the pulse repetition frequency of the system. Another important feature of the transmitter is its stability in time. For a pulse generator it is primarily the variation in time between the external trigger and the start of the transition that has to be as small as possible. This delay uncertainty is also called jitter (Fig. 2-16).
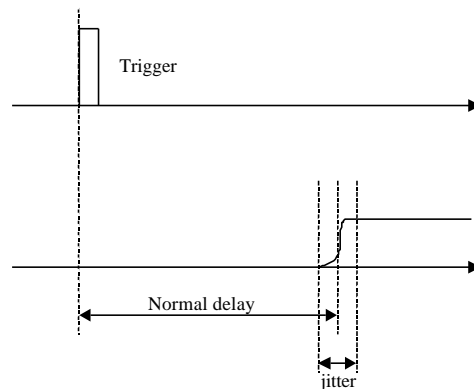

Fig. 2-16: Delay uncertainty or jitter

A good overview of different impulse generators is found in [10].

The receiver

From the hardware point of view, the receiver is the most difficult block to build. Its performance has a direct impact on the over-all system performance. The receiver has to be very sensitive, posses a large fractional bandwidth, a large dynamic range and a good noise performance. In Fig. 2-17 we show the block diagram of the receiver. From the left to the right we have a time-varying gain (TVG) amplifier, a low noise amplifier (LNA), a sample and hold circuit (S/H) and an analog-to-digital converter (A/D converter). In the following, a brief description of the blocks will be given.
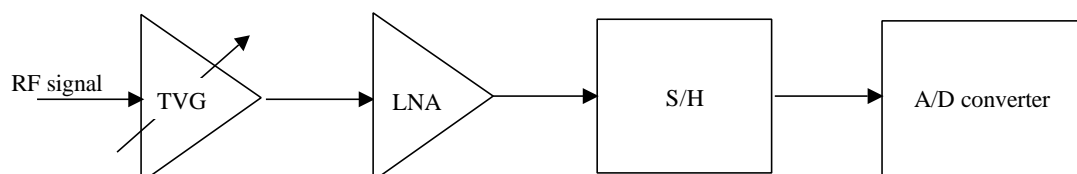

Fig. 2-17: Block diagram of receiver

(a) A/D conversion

With today's technology, conventional A/D converters like a flash converter or Sigma-Delta converters are limited to conversion rates of about 200 MHz for a 8 bit conversion and 10 MHz for a 16 bit conversion. As the received signals in GPR systems are in the frequency range of some GHz, it is impossible to use a standard A/D converter to sample the received echoes in real time, in order to respect Shannon's theorem. The solution is to slow down sampling rate by a stroboscopic or sequential sampling technique. The principle of sequential sampling is represented in Fig. 2-18. The timing control circuit of a sequential sampler is based on two ramp signals: a fast and a slow ramp. The position (in time) at which an A/D conversion is made is determined by the intersection of the fast and the slow ramp. The fast ramp is at the same rate as the PRF. The slow ramp is set to provide the desired number of samples in one A-scan. As the fast ramp is at the same rate as the PRF and a conversion is done on each intersection, it will take as many emitted pulses as points needed in one A-scan. Hence the number of points per A-scan and the PRF will limit the number of A-scans one can take per second. This number of A-scans has his importance. It will lead to a trade off between number of A-scans one can use to integrate the scans, in order to reduce noise, and the speed at which the antennas can be moved. With the technique of sequential sampling one can reduce the sampling rate from GHz to MHz or even kHz. To be exact, the time between two samples T_s is given by

$$T_s = T_p \pm \Delta T \tag{2. 33}$$

with $T_p = \dfrac{1}{PRF}$ and $\Delta T =$ the equivalent sampling period (see Fig. 2-18). The '$\pm$'-sign depends on the orientation of the slow ramp.
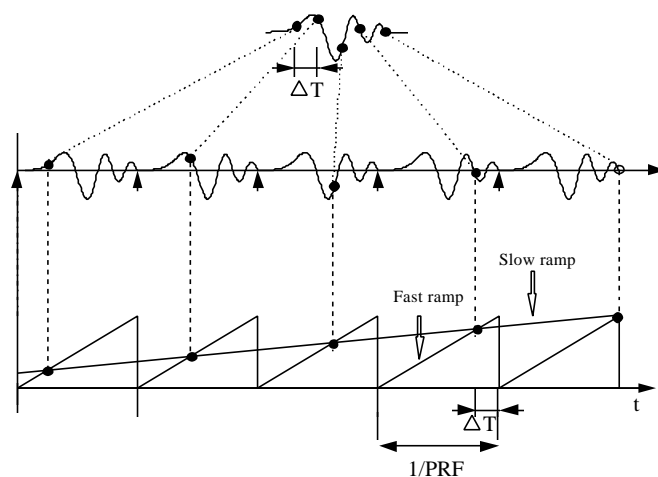
Fig. 2-18: Sequential sampling

The A/D conversion itself can be done by a conventional A/D converter. Normally 12 or 16 bits are used for conversion. A 16 bit converter will have a dynamic range of 96 dB. The dynamic range of the receiver is the ratio of the maximum detectable signal to the minimum detectable signal .

(b) Sample and hold circuit

For a correct A/D conversion the signal at the input of the A/D converter has to be stable for a certain time. The principle is that the maximum rate of signal variation must be smaller than the quantisation step of the converter during the conversion time. To provide this constant signal value to the A/D converter, a sample and hold (S/H) circuit is used.

The working principle of a S/H circuit is based on the charging of a capacitor C_s to a voltage that is proportional to the input signal so that the sample corresponds to a specific portion of the input signal.

Due to the sequential sampling the input bandwidth of the A/D converter is limited to some MHz. For the S/H circuit this is not true. The input bandwidth of this device has to be of the same order as the highest frequency in the received signal. For an UWB

system, this means that the S/H will have an input bandwidth of some GHz, which makes the design of the circuit very demanding.

In time domain GPRs, two types of S/H circuits are often found: the full-bridge sampler and the half-bridge sampler. The full-bridge sampler is commonly used in systems working with frequencies below 1 GHz. The schematic is equivalent to the schematic of a half-bridge sampler, where only 4 diodes are used in the bridge. The full-bridge sampler is characterised by a good linearity and noise performance [11]. If higher frequencies are used in a system, the preference is given to a half-bridge sampler. It has a faster response but the noise performance is worse [11]. The schematic of the half-bridge sampler is given in Fig. 2-19.
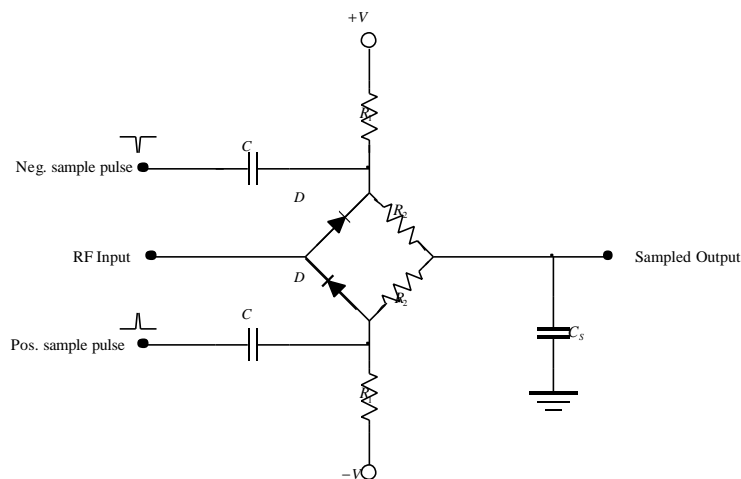

Fig. 2-19: Schematic of the half-bridge sample

The aim of the circuit is to charge the capacitor C_s to a voltage proportional to the RF input. The capacitor C_s is usually the input capacitor of an amplifier following the S/H circuit. The 2 diodes are reverse biased (blocked) by the voltages $+V$ and $-V$ during the hold status of the circuit. These voltages have to be large enough so that the RF input signal does not cause the diodes to conduct. The sampling is initiated by the 2 symmetrical and very narrow sample pulses, which will overcome the inverse bias and put the two diodes in a conducting state. During this time, the RF signal charges the capacitor C_s. As the diodes have to switch very fast from a blocked stage to a conducting stage, Schottky diodes are frequently used. For an optimum performance

of the sampler, the bridge has to be completely balanced. This means that the 2 diodes and resistors have to be matched, the two reverse bias voltages $+V$ and $-V$ have to be exactly equal and opposed in sign, and the shape of the sample pulses have to be totally symmetric. That is why S/H circuits are often implemented in hybrid ICs. The frequency response of a half-bridge sampler can be increased by using shorter sample pulses and by using diodes with a lower capacitance. These diodes however have often a higher series resistance, so both measures will increase noise.

The performance criteria of a S/H circuit are very demanding. The circuit is often designed and optimised for a specific application or system, as the S/H circuits belong to the know-how of a few companies that produce them. It is almost impossible to buy an off-the-shelf sampling head.

(c) The low noise amplifier (LNA)

Before the RF signal enters the S/H circuit, it is conditioned to make use of the whole dynamic range of the A/D converter. The signal conditioning elements consist as usual of a LNA, *i.e.* an amplifier with a very low noise figure. Remarkable about GPR receiver, as represented in Fig. 2-17, is the order of succession of the elements. The LNA is not put as first element as one would expect, but after the TVG. The explanation for this sequence is found in the utility of the time varying gain.

(d) Time varying gain (TVG)

The spherical waves radiated by the transmitting antenna and backscattered by an object are both subject to spreading loss. This means that in the far field the amplitude of the received echo of a given target decreases with R^{-2}, where R is the one-way path between the antennas and the object. Further, the objects that we are looking for are buried in a lossy medium. The deeper the object is buried, the more losses will be introduced by the ground. In other words, the later the echo appears in an A-scan, the more it will be attenuated due to these two losses. To compensate for this attenuation in function of time (or depth R), a time varying gain is introduced, giving a fixed

gain in dB per unit of time (or per meter) as represented on Fig. 2-20. The curve would approximately compensate for a loss of 50 dB/m (spreading loss + attenuation in the ground).
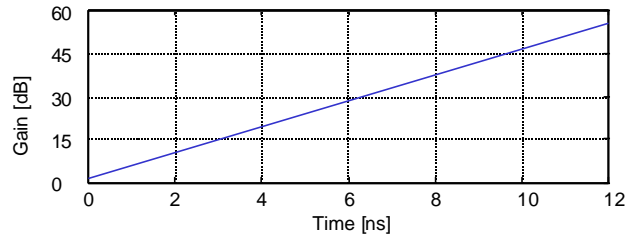

Fig. 2-20: Gain curve as a function of time

In practice the TVG is not an amplifier whose gain changes as a function of time, but an attenuator whose attenuation is changed as a function of time. The time varying attenuator is based on PIN diodes. PIN diodes have the property of having a variable resistance as a function of voltage and they have a low junction capacitance. In Fig. 2-21 a schematic is given of a TVG. Two times three diodes are put in a "T" configuration. Two different DC currents respectively forward bias the four series diodes and the two shunt diodes and hence control their dynamic resistance so that the attenuation of the input RF signal can be set.
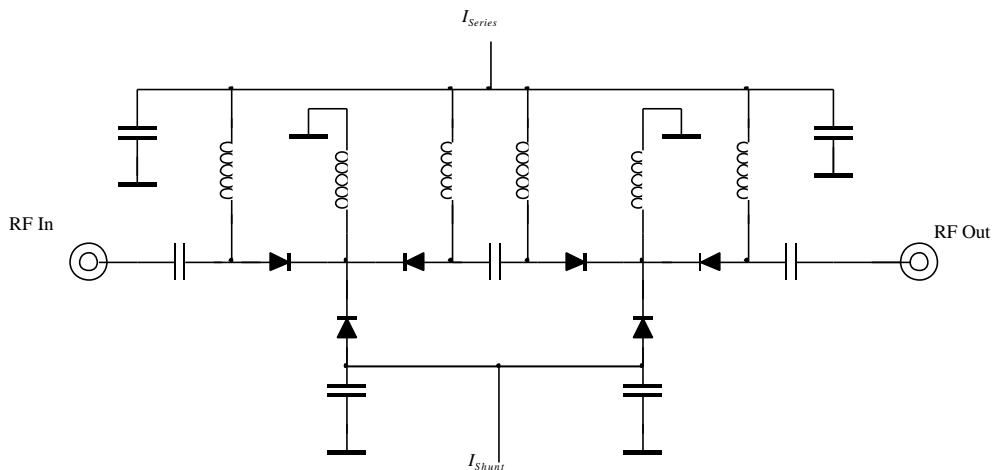

Fig. 2-21: Schematic of a time varying gain using PIN diodes

The TVG based on a time varying attenuation has an additional advantage. The first and often the largest reflection in an A-scan is produced by the air-ground interface. Reflections from objects in the ground will appear later in time and hence will be less attenuated by the TVG. By doing so, the LNA following the TVG can be designed more sensitive without saturating on the air-ground reflection. As a consequence the dynamic range of the whole receiver will increase, which would not be the case if the TVG were put after the LNA. This explains why, from the engineering point of view, it is better to put the TVG before the LNA.

Timing circuit

As explained earlier, the receiver in a time domain GPR is based on a non-coherent acquisition of the backscattered RF signal. This means that the acquisition must be controlled by a very stable and precise timing circuit that synchronises the work between the different parts in the system.

The timing circuit is responsible for mainly three things. First, it has to trigger the impulse generator. Secondly, the timing circuit has to generate the timing signals as needed for the sequential sampler, *i.e.* a trigger for the A/D converter at the intersection of the fast and the slow ramp. Third, it has to control the timing for the TVG.

The stability of the timing circuit is characterised by its time jitter, *i.e.* the uncertainty in time or the random deviation in time of its normal value. Although the sampling is slowed down by the sequential sampling, we obtain a sample of the input RF signal every ΔT (see Fig. 2-18), with ΔT in the order of some ps, so great care has to be taken to limit the time jitter of the receiver part. As a rule of thumb, one can say that system jitter has to be at least less than $\Delta T / 2$ to clearly separate two successively samples (see Fig. 2-22).
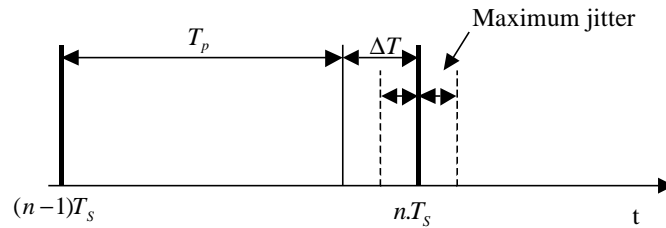
Fig. 2-22: Maximum time jitter

For example, a GPR takes 500 points in a time window of 10 ns (which corresponds to an equivalent sample period ΔT of 20 ps). The system jitter has to be less than 10 ps, which is a severe and hard to obtain condition.

There exist integrated circuits that generate the necessary timing signals for a sequential sampler. The AD9500 from Analog Devices is such a programmable delay generator. The delay is selected through an 8 bit code. The resolution of the delay is as small as 10 ps and the delay uncertainty or jitter is also typically 10 ps.

Some design parameters

In the design of a time domain GPR, there are certain parameters that can be set as a function of the application. In the following part we discuss several of these parameters. It is important to understand the influence of the parameters on the data and the acquisition time as in commercial systems they can generally be set by the user.

(a) Frequency range

The choice of the central frequency and of the bandwidth of the GPR is an important issue, and depends primarily on the type of application. For each application a set of frequency constraints can be developed. The parameters influencing the frequency range are: the size of the object, the wanted depth resolution, the maximal penetration depth, and the properties of the soil.

The basic criterion for depth resolution is that the spatial separation between two events (discontinuities in dielectric constant) must be equal to the spatial half-width of the incident pulse. Notice that the half-width in this definition has to be considered in the ground, where the velocity of propagation v is smaller than in free space, so that the pulse width in the ground is smaller than in free space. The depth resolution is given by (1.1). In Table 2.3, depth resolution is given for a mono-cycle GPR in two different kinds of ground: respectively with a e_r of 4 (sandy dry soil) and 15 (sandy wet soil). In the case of a mono-cycle the pulse-width is 1/fc.

Central frequency	Pulse-width	Depth resolution	
		$e_r = 4$	$e_r = 15$
500 MHz	2 ns	15 cm	7.7 cm
1GHz	1 ns	7.5 cm	3.9 cm
2GHZ	0.5 ns	3.75 cm	1.9 cm
3GHz	0.33 ns	2.5 cm	1.3 cm

Table 2.3: Depth resolution versus central frequency

In conclusion, for good depth resolution, short pulses are needed, which means larger bandwidth.

In Section 2.2.3 we saw that the depth of penetration strongly decreases for higher frequencies in a given soil. The electrical properties of the soil together with the wanted maximum depth penetration imply an upper limit for the used frequencies. Once frequencies above 1 GHz are used, depth penetration decreases dramatically. So if large penetration depth is needed, lower frequencies are preferred.

Besides depth resolution and attenuation, there is also the problem of clutter. Clutter can be defined as backscattered signals that are not from possible targets of interest, but occur in the same time window and have similar spectral characteristics. The smaller the wavelengths in the emitted pulse the larger the quantity of possible clutter sources in the heterogeneous ground. As a general rule it is desirable that the wavelength of the central frequency in the ground of the GPR is ten times larger than

the size of the heterogeneities in the ground to reduce clutter. This also sets a constraint for high frequencies.

(b) Time window

The time window represents the zone of interest that is to be sampled or in other words, the duration of one A-scan. The beginning and the duration of the timing window can be set by the slow and the fast ramp timing signals.
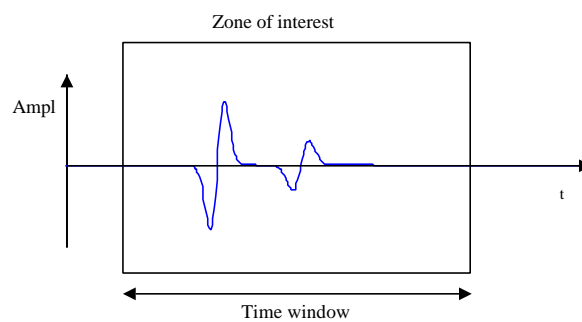
Fig. 2-23: The time window

In the application of antipersonnel mine detection the zone of interest is the top layer of the ground, between 0 and 20 cm of depth. The duration of the time window T_g is in direct relation with the maximal depth of investigation $s_{\max}$ by

$$s_{\max} = \frac{v.T_g}{2} \qquad \textbf{(2. 34)}$$

The problem is that the velocity of propagation depends on the permittivity of ground. The velocity of propagation in the ground is approximately given by (2.28). In the next Table some worst case values of T_g are represented in function of $s_{\max}$ for a velocity of propagation of c/5.

s_{max} (cm)	T_g (ns)
18	6
30	10
60	20

Table 2.4: Maximal depth of investigation

As AP mines are not deeper than 20 cm, a time window of 10 ns must be sufficient.

(c) Equivalent sampling period

The equivalent sampling period indicates the period at which one would have to sample with a conventional A/D converter. In the case of a sequential sampler, the equivalent sampling period is ΔT. In order to do an acquisition without any loss of information one has to respect Shannon's theorem. This means that the equivalent sampling frequency ($=1/\Delta T$) has to be at least twice the highest significant frequency in the emitted signal. In practice however the equivalent sampling frequency is taken much higher than two times the highest significant frequency in the emitted pulse. Typical values of ΔT in GPR applications are 10 -100 ps.

(d) Pulse Repetition Frequency (PRF)

In classic air radar, the PRF is limited by the maximal range at which one wants to detect targets, *i.e.* the maximum unambiguous range. Indeed all echo's from possible targets must be returned before the next pulse is emitted by the radar, otherwise the interpretation of range is incorrect. In GPR technology this is not really a problem. The maximum depth of investigation in the ground is usually limited by the attenuation of the ground and as a consequence will put no restriction on the choice of the PRF. In practice the PRF will be limited by the transmitter technology.

A sequential sampler takes one sample after each emitted pulse, so the PRF will influence the acquisition time of one A-scan. The PRF will also determine the mean power of the GPR pulse generator for a given peak power. Typical values of PRF are

100-1000 kHz. If 512 points are acquired per A-scan, the acquisition of one A-scan would take between 5.12 ms and 0.512 ms.

(e) Averaging or stacking

In general the noise in the received signal can be reduced by averaging (also called stacking) a number of A-scans. Averaging S A-scans means a noise reduction in amplitude by $\sqrt{S}$ or an improvement of the signal to noise ratio (SNR) by $10\log(S)$.

Normally the stack number S can be set during acquisition or stacking can be done off-line. When setting the stack number during acquisition, the GPR will automatically output an A-scan which is the average of S A-scans. Choosing S too high will considerably slow down acquisition, as well as the maximum displacement speed of the radar for a given grid (or resolution) on the ground. Typical values of S in GPR applications are 8 - 32, depending on the amplitude of the emitted pulse.

2.3. GPR in demining applications

2.3.1. State of the art

A brief summary of the state of the art in GPR development for minedetection is presented here. Land mine detection and unexploded ordnance (UXO) detection were always of major interest for the GPR research community, since GPR can inherently detect non-metallic as well as metallic objects in the subsurface. The U.S. army already sponsored efforts in this area since the beginning of the seventies. The first use of a GPR in a post conflict situation was reported by the British army after the Falkland war. The attempt however was abandoned because the operational requirements were not fully established. This failure did not discourage the military nor the scientific community to continue research in the area. The difficulty of detecting AP landmines with a GPR may not be underestimated. The size of the

objects is extremely small and the surrounding media can be very complex and rough. Furthermore, the requirements for a mine detector are severe and difficult to meet (see Preface). Therefore the GPR is more and more considered as a complementary sensor to the metal detector to reduce the false alarm rate of the latter and not as a stand-alone detector. There exists already systems which integrate those two types of sensors and which look close to commercialisation. An example of this is the DIGS. DIGS is a handheld wide band stepped frequency GPR, with automatic target recognition algorithms, which is "pluggable" into a standard Schiebel metal detector. A more recent example is the HSTAMIDS, which is a handheld mine detector developed for the U.S. Army and also combines a GPR and a metal detector. In the project planning, the first unit has to be equipped by 2004. The main problem with these types of (army-linked) projects is that it is very hard to get feedback on the performances of the systems.

In Europe there are a lot of governmental (military) and academic research groups doing research on the use of GPR as an AP Landmine detector. Some examples are:

− the Netherlands Organisation for Applied Scientific Research (TNO) [12], who is developing in the scope of the HOM2000 Project a demonstrator for humanitarian demining, combining MD, GPR, IR and vapor detection

− the French-German Research Institute of Saint-Louis (ISL)

− the Defence Evaluation and Research Agency (DERA) in the UK [13]. DERA is working for instance on the integration of a MD, UWB GPR and nuclear quadrupole resonance (NQR) in one sensor (AHHMD project). They also develop the UWB GPR in the project Mineseeker and developed recently a GPR system with an antenna array (4 by 7 bow-tie antennas)

− the Sweden's Defence Research Establishment (FOA) working on metal detector, ground penetrating radar, optical sensors and demining canines [14]

− the Delft University of technology (TU Delft), with departments as IRCTR and ITS which are very active in the domain of GPR and humanitarian demining [15]

− the Norwegian University of Science and Technology where research is done on a stepped frequency GPR for landmine detection [16].

Further almost all ESPRIT projects of the European Commission on humanitarian demining, like Minerec, Demine, Dream, Infield, Hope, Pice and Lotus, include a GPR in their single- or multi-sensor system [17]. The results of the projects are expected for 2001. In Belgium there is besides the RMA [18] also the VUB [19] where research on the use of GPR for AP Landmine detection is undertaken. There are probably more GPR mine detection research groups in Europe than described here. The ones mentioned, are the research groups and projects with whom we have connections.

The literature concerning GPR mine detection is quite extended and all recently written. The main papers describing the use of GPR, the problems and achievements in mine detection, are found in proceedings. First there are of course the conferences that are totally dedicated to Humanitarian demining like the IEE conferences on the detection of abandoned Landmines in October 1996 and 1998, the Mine '99 conference in Florence (It) in 1999, the SusDem conference in Zagreb in Sep. 1997. Recently almost all big conferences in the domain of Electro-Magnetic and Antennas and Propagation and of course the specialised GPR conferences, like the biannual International Conferences on GPRs include special sessions on humanitarian demining.

2.3.2. Field trials and conclusions

In order to test and evaluate different sensors or systems, we installed in collaboration with the Army Forces Bomb Disposal Unit, two test sites: a little one at the Royal Military Academy (RMA) and a larger but still structured one in Meerdaal (near Leuven). The RMA test field contains only 7 AP mines and 6 mine-like targets (can, brick, stone,..) and is mainly for experimental purposes. In Meerdaal we have four identical test fields of 9m by 5m. Each of the four fields contains a different soil type: sand, gravel, local ground (37% sand, 53% silt, and 10% clay) and a mixture of the three previous. In Fig. 2-24 a plan of the test site is given. In Fig. 2-25 one of the four identical test fields is shown in detail. The position of each target is indicated by

wooden pickets around the field (A-D,1-8). The depth of the AP mine depends on its position in the field. The AP mines at position A5, B5 and C5 have a tilt angle of 45°.
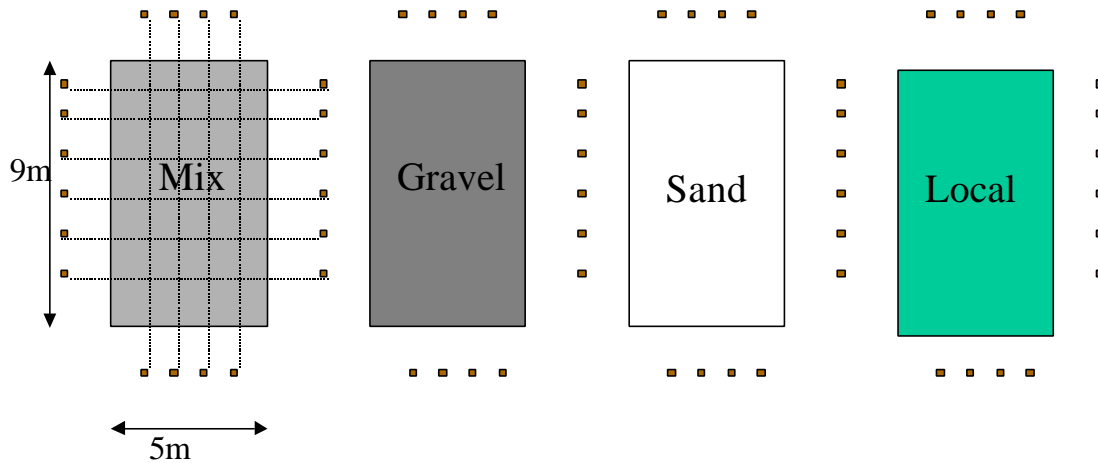

Fig. 2-24: Plan of test field in Meerdaal
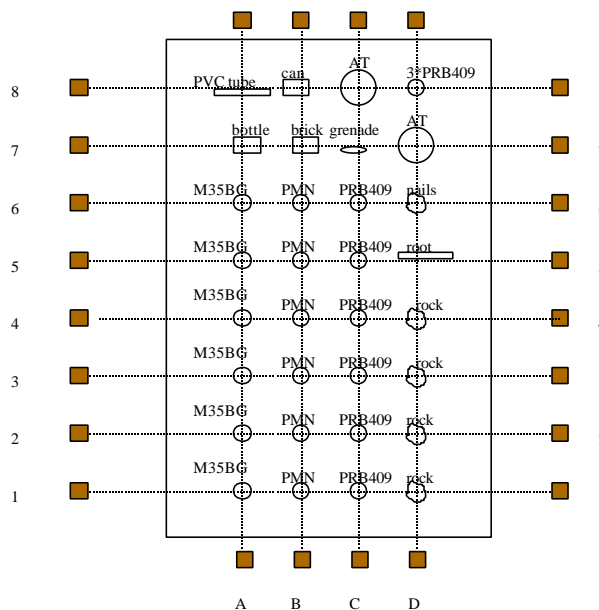

Fig. 2-25: Detailed plan of one test field

The Meerdaal test minefields was laid in the spring of 1997. The now more than three years old test field is considered as a good intermediary stage between laboratory conditions and a real mine field. The field is still structured, but the position of the objects is only approximately known, as probably some objects have moved

throughout the years. Furthermore the subsurface of most of the fields is cluttered and the surface in some places can be rough and covered with vegetation. Three different types of AP mines are found in these test fields: the former Soviet PMN mine and two Belgian AP mines the M35BG and the PRB409. The three mines are shown in Fig. 2-26, more details on their dimensions are found in table 2.5. The PMN and the PRB409 are drill mines. The M35BG is made inert by the demining service itself. The primary explosive in the detonator and the TNT have been replaced by a silicone, RTV 3110 from Dow Corning. In the table 2.6 the most important properties relevant for GPR and IR of both the TNT and the silicone are compared.

Fig. 2-26: From left to right: PMN AP mine, M35BG AP mine and the PRB409 AP mine

	Radius [mm]	Height [mm]	Explosive
PMN	112	56	200 gram of TNT
M35BG	63.5	38	100 gram of TNT/KNO3
PRB409	82	28	80 gram of trialene

Table 2.5: Technical details on the AP mines used in the test field

	TNT	Silicone
Density (g/cm³)	1.56	1.17
Dielectric constant at 1GHz	2.89	2.89
loss angle at 1GHz	0.003	0.006
Thermal conductivity W/(m.K)	0.33	0.35
Specific heat cal/(g.°C)	0.234	0.2

Table 2.6: Properties of TNT and silicone

On these test fields, we did several field trials with commercially available GPR systems. The systems we tested are the RAMAC 1GHz, the GSSI SIR-2 with the 1GHz horn antenna , GSSI SIR-2 with the 2.5GHz horn antenna and the ERA with the 1GHz and 2GHz antenna. All of these systems are time domain GPRs. It was not our intention to compare the different GPR systems; we only wanted to gain experience in the use of GPR in this particular application.

The data from the commercially available systems were analysed. In short the following conclusions were drawn.

− The antennas are a critical point. In three out of the five tested systems, the antennas were designed to be in contact with the ground. The antennas coupled to the ground turned out to have a low degree of mobility in a rough and with vegetation covered scene. Two out of the five tested systems had horn antennas, which could be used off-ground. The antennas however were so big and heavy that they were unmanageable in the field. To give an idea of their dimensions, the 2.5 GHz horn antenna, which is the smallest of the two horn antennas, was still 60 cm by 22 cm by 32 cm.

− In the field it is difficult to detect small objects. The antennas must be used in a systematic scan pattern, in order not to miss any spot of the scanned area. If the antennas passed just besides a target, the target was in most of the cases not detected.

− Conventional GPR systems have a poor classification rate. With the bare eye, no difference could be made between a mine-like target and an AP mine.

Furthermore, targets which were shallowly buried or buried flush with the ground were masked by the large air-ground interface reflection. If the air-ground interface was smooth and flat, it was possible to retrieve the targets in the image by simple image processing techniques. But when the air-ground interface was too rough, these simple image-processing techniques failed. Obviously there is a lack of depth resolution in the conventional GPR systems.

2.4. Summary

In this chapter a general description of the conventional GPR is given. The history of the GPR, the different types of GPRs and the physics behind the propagation of electromagnetic waves in a lossy dielectric are discussed. Important to keep in mind for the application is that the attenuation of the electromagnetic waves in a lossy soil increases both with frequency and moisture content of the soil. In a second part of the chapter the state of the art in demining applications, the description of the test fields and the conclusions of the field trials with commercially available systems are presented. The test revealed that the choice of the central frequency and the bandwidth of the GPR are an important issue. Classical GPRs are mostly designed for geophysical applications and use central frequencies below 1GHz. As landmines are small objects and are buried close to the air-ground interface, a larger bandwidth is needed for a better depth resolution and detailed echo. This means the use of an ultra-wideband (UWB) GPR imposes itself. It can be expected that a larger bandwidth also will enhance the classification rate of the GPR. On the other hand, using an ultra-wideband system involves inevitably the use of higher frequencies. These higher frequencies will be strongly attenuated by the lossy soil as shown in this chapter. Furthermore, the use of a large bandwidth has his implications on the hardware of the GPR system. Although the UWB GPR seems a promising sensor for the demining application, the advantages of the ultra-wideband GPR over a conventional GPR and the drawbacks of the use of higher frequencies have to be well balanced against each other.

Therefore we decided to develop a time domain UWB GPR to study its advantages and limitations. The choice of a time domain system over a stepped frequency system was mainly influenced by the fact that a lot of equipment and know-how on UWB time domain systems was already present in our laboratory. In the next chapter we will concentrate on the development of UWB GPR antennas. If we want to use the UWB GPR for the demining application, the antennas have to meet some particular specifications.

REFERENCES

[1] W. Stern, "Uber Grundlagen, Methodik und bisherige Ergebnisse elektrodynamischer Dickenmessung von Gletschereis," *Z. Gletscherkunde*, vol. 15, pp. 24-42, 1930.

[2] R. M. Morey, "Continuous subsurface profiling by impulse radar," *Proceedings of the Engineering Foundation Conference on Subsurface Exploration for Underground Excavation and Heavy Construction*, pp. 213-232, Aug. 1974.

[3] D. J. Daniels, D. J. Gunton and H. F. Scott, "Introduction to subsurface radar," *IEE Proceedings*, vol. 135, no.4, pp. 278-320, Aug. 1988.

[4] D. J. Daniels, *Surface Penetrating Radar*. London: IEE, 1996.

[5] OSD/DARPA, Ultra-Wideband Radar Review Panel, *Assessment of Ultra-Wideband (UWB) Technology*. Arlington: DARPA, 1990.

[6] D. A. Noon, *Stepped- frequency radar design and signal processing enhances ground penetrating radar performance*, Doctoral thesis, University of Queensland, AU, 1996.

[7] M. Storme, I. Huynen and A. Vander Vorst, "Characterization of wet soils in the 2-18 GHz frequency range," *Microwave and optical technology letters*, vol. 21, no. 5, June 1999.

[8] A. von Hippel, *Dielectric materials and applications.* Boston: Artech House, 1995.

[9] G. Turner and A. F. Siggins, "Constant Q attenuation of subsurface radar pulses," *Geophysics*, vol. 59, no. 8, pp. 1192-1200, Aug. 1994.

[10] M. Piette, *Banc de mesure en régime transitoire de la signature radar d'objets tridimensionnels*, Doctoral thesis, Université catholique de Louvain and Royal Military Academy, Belgium, Oct. 1995.

[11] W. Murray, C. Lewis, Z. Yang and J. T. A. Pollock, "Development of high resolution GPR hardware in the frequency range 300 MHz - 3.5 GHz," *Sixth International Conference on Ground Penetrating Radar*, Sendai, Japan, pp. 505-510, Sep.-Oct. 1996.

[12] http://www.tno.nl/cases/defensie/humanitair_ontmijnen.html

[13] http://www.dera.gov.uk/

[14] http://www.foa.se/

[15] http://irctr.et.tudelft.nl/

[16] Egil Eide, *Radar imaging of small objects closely below the earth surface*, Doctoral thesis, Norwegian University of Science and Technology, Norway, Aug. 2000.

[17] http://www.cordis.lu/esprit/src/hphdrtd.htm

[18] http://www.sic.rma.ac.be/Projects/Hudem/

[19] http://www.etro.vub.ac.be/